Ultrahigh vacuum deposition of CdSe nanocrystals on surfaces by pulse injection

2004 J. Phys.: Condens. Matter 16 7565

(http://iopscience.iop.org/0953-8984/16/43/001)

INSTITUTE OF PHYSICS PUBLISHING JOURNAL OF PHYSICS: CONDENSED MATTER

J. Phys.: Condens. Matter **16** (2004) 7565–7579 PII: S0953-8984(04)82082-4

Ultrahigh vacuum deposition of CdSe nanocrystals on surfaces by pulse injection

R Bernard[1], V Huc[2], P Reiss[3], F Chandezon[3], P Jegou[4], S Palacin[4], G Dujardin[1] and G Comtet[1]

[1] Laboratoire de Photophysique Moléculaire, Bâtiment 210, Université de Paris-Sud, 91 405, Orsay, France
[2] Laboratoire de Chimie Inorganique, Bâtiment 420, Université de Paris-Sud, 91 405, Orsay, France
[3] Département de Recherche Fondamentale sur la Matière Condensée, CEA Grenoble 17, rue des Martyrs, 38054, Grenoble, France
[4] Chimie des Surfaces et Interfaces, CEA Saclay, Bâtiment 466, 91191, Gif sur Yvette, France

Received 14 June 2004, in final form 2 September 2004
Published 15 October 2004
Online at stacks.iop.org/JPhysCM/16/7565
doi:10.1088/0953-8984/16/43/001

Abstract

The fabrication of thin films of colloidal semiconductor nanocrystals is attracting much attention due to their exceptional optoelectronic properties. This requires the development of new methods for depositing nanocrystals under well-controlled conditions. Here, we report the use of the pulse injection method to deposit CdSe nanocrystals under ultrahigh vacuum (UHV) on clean and well-ordered surfaces. The deposition of nanocrystals has been tested by x-ray photoelectron spectroscopy (XPS) and near edge x-ray absorption fine structure spectroscopy. Special attention has been paid to the preparation of very pure solutions of CdSe nanocrystals using cadmium stearate, trioctylphosphine oxide (TOPO) and the TOP/Se adduct for the nanocrystals synthesis followed by dissolution in pentane. It has been found that CdSe nanocrystals adsorb with similar sticking coefficients on graphite, hydrogenated silicon (100) and hydrogenated diamond (100) surfaces. Furthermore, the XPS analysis has revealed that the surface of the CdSe nanocrystal is Cd rich, which has important consequences for the optical and chemical properties. This ability to deposit semiconductor nanocrystals under UHV conditions on clean and well-ordered surfaces opens up new perspectives for studying in a reliable manner all their chemical, electronic and optical properties.

1. Introduction

Semiconductor nanocrystals prepared by colloidal synthesis exhibit a number of interesting properties for building electronic [1] and optical [2–10] devices. Extensive experimental [11–16] and theoretical work [17] has been done in particular on the electronic transport properties

of double-barrier tunnel junctions formed by a single colloidal nanocrystal between the tip of a scanning tunnelling microscope (STM) and a surface. However, this electronic transport depends crucially on the electronic coupling between the nanocrystal and the surface. Therefore, the electronic and chemical properties of the surface need to be very well defined, thus requiring deposition of the nanocrystal on clean and well-ordered surfaces. In previous studies using organic solutions of nanocrystals, a drop of the liquid was deposited at ambient conditions onto the surface [11–14], or the surface itself was immersed in the solution [15]. Other studies have used electrodeposition [15, 16], with the substrate immersed in the electrolyte. In all these studies, the surfaces have been in prolonged contact with the solution, resulting in dirty and disordered surfaces.

Here, we present a new method for nanocrystal deposition under ultrahigh vacuum (UHV) conditions on clean and well-ordered surfaces. An important prerequisite for such nanocrystal deposition in a clean and well-controlled environment is to prepare very pure solutions of nanocrystals to prevent co-deposition of any chemical contaminant. In the first part, we will describe a modified synthesis method required for the preparation of the pure solutions of CdSe nanocrystals. In a second part, we will describe the pulse injection method for nanocrystal deposition. This method has been previously used to deposit biological molecules on Cu(111) [18, 19] and carbon nanotubes on H-terminated Si(100) surfaces [20]. We will show that this method can be applied to deposit nanocrystals under UHV conditions on clean highly oriented pyrolytic graphite (HOPG) and hydrogenated Si(100) and C(100) surfaces. Semiconducting surfaces (Si(100)), and in particular wide band gap semiconductor surfaces (C(100)), are of particular importance for exploiting the optoelectronic properties of nano-objects [21]. The deposited nanocrystals have been analysed by x-ray photoelectron spectroscopy (XPS) and near edge x-ray absorption fine structure (NEXAFS) spectroscopy. It has been shown that the nanocrystals have similar sticking coefficients on the three surfaces studied. In the case of nanocrystals deposited on a graphite surface, a detailed analysis of the XPS spectra, involving analytically calculated attenuation factors, has enabled the chemical composition to be deduced, i.e. the relative number of Cd and Se atoms, for the nanocrystal surface. This relative number has very important consequences on the optical and chemical [22, 23] properties of the nanocrystals.

2. Experimental details

2.1. Synthesis and characterization of semiconductor nanocrystals

Although the synthesis of high quality CdSe semiconductor nanocrystals is now well described in the literature [24–26], we have modified the existing synthesis procedures in order to meet the specific requirements of our experiment. Indeed, even trace amounts of contaminants along with nanocrystals in the solution may contaminate the surface and modify its electronic properties. This prompted us to re-examine the existing synthesis procedures, keeping in mind the purification of the nanocrystal solution rather than the monodispersity of the nanocrystals.

The well-known ‘cadmium salt’ method [25, 26] has been chosen as a starting point, due to the accessibility of the reagents, and the quality of the resulting nanocrystals. Our initial attempts with phosphonic acids [25–27] were unsuccessful. Although good optical quality nanocrystals were obtained in this latter case, the complete removal of unreacted phosphonic acids and/or cadmium phosphonate proved to be very difficult. Subsequently, the growth of 3 nm diameter CdSe nanocrystals starting from cadmium acetate as a precursor proved to be quite difficult to control. With cadmium salts such as stearates or phosphonates as the cadmium source, it has been shown that long chain primary or secondary amines have a beneficial effect on the growth and the size distribution of the nanocrystals [28]. Unfortunately,

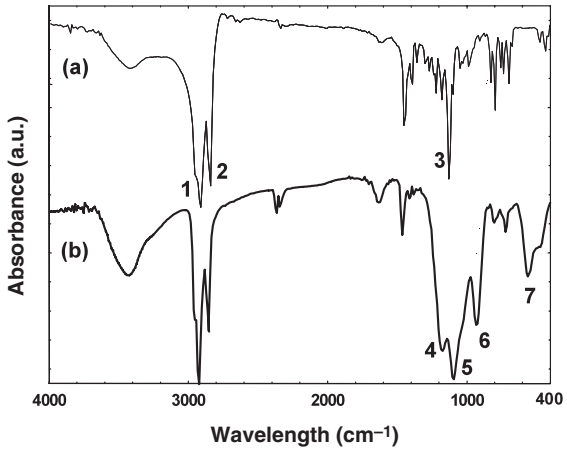

Figure 1. Room temperature FTIR spectra: (a) TOPO dispersed in KBr; bands 1 and 2 are associated with the C–H stretch, and band 3 with the P–O stretch; (b) CdSe nanocrystals dispersed in KBr; bands 4, 5 and 6 are associated with the P=O stretch and band 7 with the P–Se stretch.

although high quality nanocrystals were obtained, these amines proved to be quite difficult to remove completely from the solutions and reduction in the fluorescence of the nanocrystals was observed. These reagents were thus not used for our synthesis.

The synthesis procedure that we have chosen (see appendix A for details) involves cadmium stearate (synthesized from stearic acid and cadmium oxide), trioctylphosphine oxide (TOPO) and the trioctylphosphine (TOP)/Se adduct (plus toluene) as reagents. In order to control the growth of the nanocrystals, the concentration of the reagents has been decreased compared to the amine-based procedures. Although the growth of the nanocrystals is fast, 3 nm nanocrystals have been reproducibly obtained and easily purified. The purity of the nanocrystal solution has been checked by means of nuclear magnetic resonance (NMR), using a Bruker AC 250 spectrometer, and by Fourier transform infra-red (FTIR) spectroscopy, with a Perkin-Elmer FTIR-1000 spectrometer. In the latter case, the expected C–H bands and three different groups of P=O bands are observed (see figure 1) indicating the presence of at least three different coordination sites of the TOPO ligands on the surface of the nanocrystals. A comparison with the FTIR spectra of nanocrystals obtained by the dimethylcadmium method [29], where only two P=O bands are observed, shows that some differences may exist between the surfaces of nanocrystals synthesized according to different procedures. From the examination of these P=O bands, no free TOPO ligand is observed. This is confirmed by a test experiment where increasing amounts of TOPO are added to the nanocrystal powder (see figure 2) resulting in the appearance of the very sharp 1145 cm^{-1} band in the FTIR spectrum characteristic of unbound TOPO ligands. FTIR spectroscopy also shows the absence of the characteristic bands of the starting products stearic acid and cadmium stearate at 1702 and 1540 cm^{-1} respectively [30]. A broad band is also observed at 560 cm^{-1} (figure 1). This band (not observed in the FTIR spectra of pure TOPO) is assigned to the P=Se bond[5]. FTIR spectroscopy thus directly confirms the presence of TOPSe ligands on the surface of the crystals. NMR spectroscopy also confirms the absence of free ligands in solution, as the sharp bands associated with free TOPO are not observed [31].

[5] It should be noted that in the case of phosphonic acid-based synthesis, the presence of unreacted acid or cadmium phosphonates is difficult to control, due to the strong overlapping with the P=O bonds of TOPO ligands bonded to the surface of the nanocrystals.

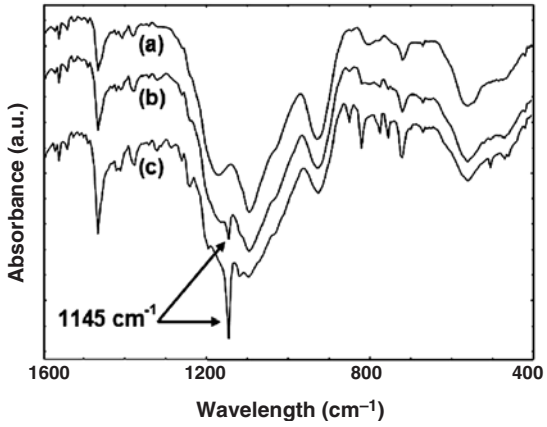

Figure 2. Room temperature FTIR spectra: (a) nanocrystals dispersed in KBr; ((b) and (c)) nanocrystals dispersed in KBr upon addition of increasing amounts of TOPO.

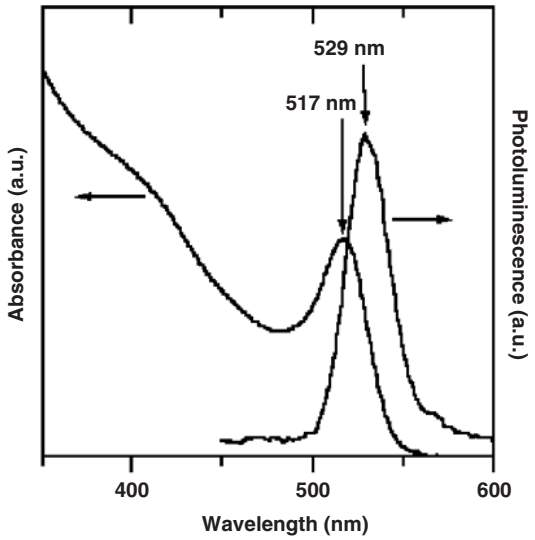

Figure 3. Room temperature absorption and photoluminescence spectra of the CdSe nanocrystals used in the pulse injection deposition. The nanocrystals are dispersed in heptane and the excitation wavelength of the luminescence is 340 nm.

The nanocrystals have also been characterized via their absorption and photoluminescence spectra (see figure 3) after dispersion in hexane. The main band at 517 nm indicates an average diameter of about 3.0 nm [24]. The shape and width of the absorption and photoluminescence bands indicate that the monodispersity of our synthesized NC is comparable to the one in [24].

2.2. Deposition methods

We have tested two separate methods for depositing the semiconductor nanocrystals on surfaces under ultrahigh vacuum (UHV) conditions.

The first method is the so-called 'filament method' which has been previously applied for the deposition on surfaces of large organic molecules [32]. In this method, a tungsten filament,

on which a droplet of toluene solution containing the nanocrystals has been deposited, is introduced in the UHV chamber and placed in front of the surface. The filament is heated to evaporate the nanocrystals and cause them to adsorb on the surface. This 'filament method' differs from standard evaporation methods using evaporation cells in that here, the heating of the filament can be pulsed, thus increasing the evaporation of the chemical products relative to their dissociation [33].

The second method is the pulse injection method, which has been previously used for depositing biological molecules [17, 18] and carbon nanotubes on surfaces [19, 20]. A solution of nanocrystals in pentane is introduced through an electromechanical valve, which is connected to the UHV chamber. The initial pressure in the UHV chamber is lower than 3×10^{-10} mbar. The sample is placed in a horizontal position 1 cm below the pulse valve. The valve is opened for a short time, typically 5 ms, so a droplet of a solution of pentane containing the nanocrystals is introduced in the UHV chamber. During the pulse opening of the valve, the pressure rises to 1×10^{-5} mbar and recovers within 30 s. This ensures that the exposure of the surface to pentane will be relatively low (about 10^{-4} L). If the surface, as is the case here with HOPG, hydrogenated Si(100) and hydrogenated C(100) surfaces, is non-reactive to pentane, there will be no effect of the pentane exposure on the surface. It follows that the surface will behave exactly as if it was kept under ultrahigh vacuum conditions throughout the experiment.

2.3. Core electron spectroscopy

Core electron spectroscopy experiments have been performed by using either an x-ray source or the synchrotron radiation source, SuperACO, in Orsay. In this latter case, near edge x-ray absorption fine structure (NEXAFS) studies around the C 1s level have also been performed. While core electron spectroscopy has enabled the detection of the atomic species present on the surface after nanocrystal deposition, NEXAFS studies have been used to evidence the presence of the carbon chains on graphite and diamond.

The UHV experimental set-up for sample preparation and photoelectron analysis has been described elsewhere [34]. Preliminary studies on a polycrystalline CdSe sample have been performed to determine the optimum photon energy (600 eV) for detection of photoelectron signals from the 4d and 3d core levels of Cd and the 3d and 3p core levels of Se. In all these studies, the photon beam impinges at a grazing angle of 63.5° onto the sample in order to further improve the surface sensitivity. Detected photoelectrons are emitted at 26.5° from the normal of the sample. The energy window of the electron analyser is 70 eV for photoemission studies and 100 eV for NEXAFS studies. The overall resolution of the photoemission bands is 3 eV. The photon energy has been calibrated using the C 1s photoemission band at 284.5 eV (283.5 eV) in the case of the graphite (diamond) surface and the Si 2p photoemission band at 99.6 eV in the case of the silicon surface [35]. NEXAFS experiments around the C 1s excitation threshold have been recorded in the partial electron yield mode, by detecting Auger electrons of 243 eV [37]. In the case of graphite, NEXAFS spectra around the C 1s absorption threshold have been calibrated by setting the observed C(1s) π^* resonance at 285.5 eV [36]. In the case of hydrogenated diamond, NEXAFS spectra have been calibrated using the second absolute band gap of diamond at 302.4 eV [38].

3. Results

3.1. Deposition by the filament method

For this first experiment, we have used nanocrystals synthesized by Reiss *et al* [27] in a mixed solvent containing TOPO and hexadecylamine without any specific purification. In

Table 1. Photoemission band intensities, using an Al Kα x-ray source, from a graphite surface after (*a*) deposition of a drop of a nanocrystal solution in air, (*b*) evaporating a nanocrystal solution under vacuum by using the filament method and (*c*) evaporating a TOPO solution under vacuum by using the filament method. The nanocrystals used in this study have been synthesized according to Reiss *et al* [27].

	Peak surface		
XPS peak	*a*	*b*	*c*
C 1s	3968.6	4468.6	2485.6
O 1s	170.7	202.8	218.0
N 1s	14.0	18.6	0
P 2p	134.8	137.0	100.3
Cd $3d_{5/2}$	236.7	0	0
Se 3d	43.2	14.3	0

order to check that the x-ray photoelectron spectroscopy (XPS) was working properly, we have deposited in air a droplet of the heptane solution containing the nanocrystals on a clean HOPG surface. The XPS analysis using an Al Kα x-ray source revealed the presence of all the nanocrystal chemical constituents, i.e. Cd, Se, P, N and O. The intensities of the most intense photoemission bands are reported in table 1. Then, we evaporated, in UHV, the same nanocrystal solution on a HOPG surface by using the filament method. The XPS analysis of the deposit revealed essentially P and O (see table 1). No noticeable signal from Se and Cd could be detected. This indicates that only the TOPO ligands that have been desorbed from the nanocrystals are deposited on the surface. To check this hypothesis, we deposited using the filament method a toluene solution containing only TOPO molecules. The XPS analysis of this TOPO molecule deposition as shown in table 1 is very similar to that obtained with the solution containing the nanocrystals. These results clearly demonstrate that the nanocrystals cannot be deposited on a HOPG surface by evaporation under UHV conditions even when using the filament method, which seemed *a priori* the most suitable method.

3.2. Deposition of nanocrystals by pulse injection

Here, we present the results of the nanocrystal deposition by the pulse injection method under UHV conditions on three different surfaces, i.e. HOPG, hydrogenated Si(100) and hydrogenated C(100) surfaces. In these experiments, we have used the nanocrystals synthesized and purified as described in section 2.1 and appendix A. The nanocrystal powder has been dissolved in pentane, which is expected to have a low chemical reactivity with the surfaces studied and to evaporate rapidly. XPS and NEXAFS analysis have been performed by using the monochromatized synchrotron radiation of Super-ACO in Orsay as a photon source of variable energy in the 150–1000 eV range.

3.2.1. Deposition of nanocrystals on graphite surfaces. The XPS spectra of the HOPG surface after the injection of 120 pulses of the nanocrystal solution under UHV are reported in figures 4(a) and (b). The photoemission bands associated with the Cd 4d, Cd $3d_{5/2}$, Cd $3d_{3/2}$, Se 3d, Se $3p_{1/2}$, Se $3p_{3/2}$, P 2p and P 2s core levels [35] are clearly seen. Moreover, Auger electrons from Cd at 379 and 385 eV kinetic energies and Auger electrons from O at 510, 489 and 473 eV kinetic energies [36] are also detected. These observations are a first indication that the nanocrystals have been properly deposited on the surface under UHV conditions. Information on the carbon chains of the ligands has been obtained by comparing

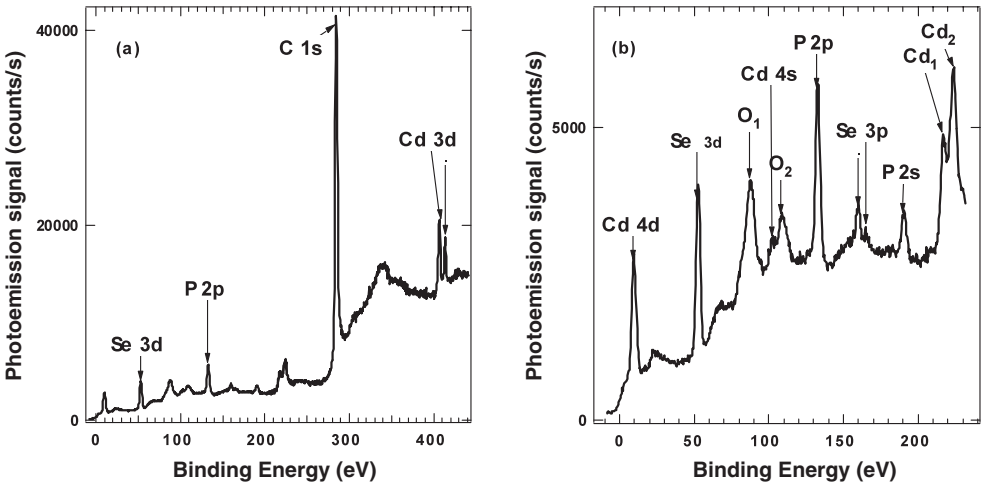

Figure 4. XPS spectra of the graphite surface after injection of 120 pulses of a CdSe nanocrystal solution in pentane under UHV. The O_1, O_2, Cd_1 and Cd_2 bands are associated with the Auger electrons of oxygen and cadmium. The photon energy is 600 eV. The angle between the photon beam and the normal of the sample is 71.5°. The binding energy extends up to 440 eV (a) and 230 eV (b).

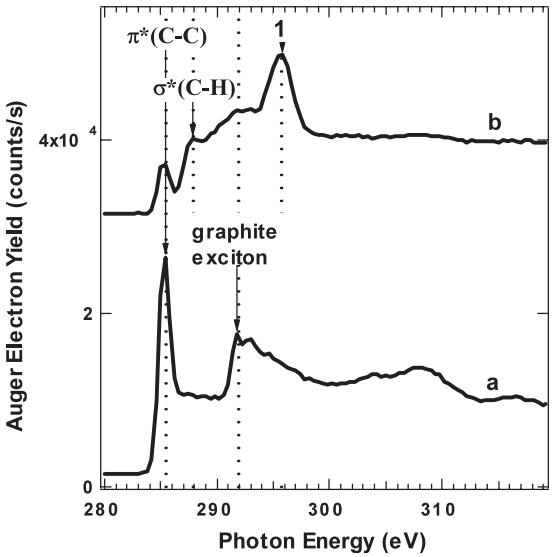

Figure 5. NEXAFS spectra of the graphite surface (a) before and (b) after injection of 120 pulses of the CdSe nanocrystal solution in pentane under UHV. The energy of the electron analyser is set up at 243 eV and the pass energy is 100 eV. The photon beam impinges at 71.5° onto the sample. The spectra have been normalized to the same photon flux. Feature 1 is the photoemission band associated with the 3d core levels of Se.

the NEXAFS spectra around the C 1s absorption threshold before and after the nanocrystal deposition (see figures 5(a) and (b)). The NEXAFS spectrum of the clean graphite surface shows the intense 1s π^* resonance at 285.5 eV [37]. After the deposition, the intensity of this feature decreases, while a feature at 287.8 eV [38], which characterizes the alkyl chain of

the nanocrystal ligands, appears. This indicates that the nanocrystals are deposited with their ligands by the pulse method.

Quantitative information on the elemental composition of the deposited nanocrystals has been obtained, from the relative intensities of the Cd 3d, Se 3d and P 2p photoemission bands, whose photoionization cross-sections at 600 eV are known [39]. The photoelectrons emitted from the Cd 3d, Se 3d and P 2p core levels have different kinetic energies and therefore different elastic mean free paths in the CdSe nanocrystals. These mean free paths are smaller than the diameter of the nanocrystals ($d = 3$ nm). Therefore, the intensity of each photoemission band is proportional to the number of emitting atoms weighted by a specific attenuation factor. Photoelectrons emitted from Cd 3d, Se 3d and P 2p core levels by 600 eV photons have kinetic energies of 296, 545 and 464 eV. Their elastic mean free paths (λ) in a CdSe crystal are 6.5, 12.45 and 11.15 Å respectively [40][6]. For simplicity, let us first assume that the nanocrystal is a cube of side d. The intensities of the Cd 3d (Se 3d) photoemission bands originating from one nanocrystal are proportional to the number of Cd (Se) atoms in the cube weighted by an attenuation factor, A_1, which depends on the mean free path and on the size of the cube as follows:

$$A_1 = \frac{\lambda}{d}\left(1 - \mathrm{e}^{-\frac{d}{\lambda}}\right).$$

For a cube with a side of 30 Å, one obtains attenuation factors of 0.22 (0.39) for Cd 3d (Se 3d) photoemission bands. The attenuation factors associated with two superposed nanocrystals are

$$A_2 = \frac{\lambda}{2d}\left(1 - \mathrm{e}^{-\frac{2d}{\lambda}}\right),$$

that is to say 0.11 (0.21) for the Cd 3d (Se 3d) photoemission bands. It follows that (i) in the case of multilayers of nanocrystals, nearly 100% of the photoemission signals comes from the top layer. We emphasize that the nanocrystals may have a non-stoichiometric surface chemical composition, i.e. the chemical composition of the surface may be different from that of the bulk. Therefore, we have calculated the attenuation factors A_S and A_B for surface and bulk atoms respectively (see appendix B). The intensity of a photoemission band is then proportional to $A_S N_S + A_B N_B$, N_S and N_B being the number of surface and bulk atoms.

The measured ratio of the Cd 3d and Se 3d band intensities in the XPS spectrum is 6.4. From this, we have estimated the Cd:Se stoichiometry in the nanocrystal. The number of Cd and Se bulk atoms in a spherical nanocrystal (diameter $d = 3$ nm) has been estimated to be 300 each from the bulk density of solid CdSe (5.66 g cm^{-3}) [41] and the molar masses of Cd (112 g mol^{-1}) and Se (79 g mol^{-1}). It follows that the mean distance, r, between atoms is about 3 Å. The number of surface relative to bulk atoms has been taken as $6\,r/d$, resulting in an estimated number of surface atoms of 250. We have calculated the ratio of the Cd 3d and Se 3d photoemission bands as a function of the number of surface Cd atoms (N_S (Cd)), keeping the total number of surface atoms (Cd plus Se) equal to 250 and the number of bulk Cd and Se atoms equal to 300 each. The attenuation factors are calculated in appendix B, and the photoionization cross-sections are those given in [34]. The best fit between the calculated and the measured Cd 3d to Se 3d ratio of the photoemission bands has been obtained when 74% of the surface atoms are Cd atoms. This yields a ratio of cadmium to selenium atoms of 1.45. The surface stoichiometry of CdSe nanocrystals has been previously investigated by different methods, such as XPS [29] as performed here, ^{31}P nuclear magnetic resonance [42] and more

[6] Values of the inelastic mean free path have been obtained from the electron inelastic mean free path database of the National Institute of Standards and Technology (NIST). The atomic weight is 191.371, the density 5.66 g cm^{-3}, the gap 2.4 eV and the number of valence electrons 18 (12 for Cd and 6 for Se).

recently the Rutherford backscattering approach [43]. Our finding of an excess of cadmium atoms on the nanocrystal surface differs from the result of Katari *et al* [29] who found equal amounts of Cd and Se atoms for nanocrystals prepared in TOPO. In our case, nanocrystals are prepared in TOPO and TOP and our results are in agreement with the ^{31}P nuclear magnetic resonance study, indicating also an excess of Cd sites relative to Se sites on the nanocrystal surface and with the recent Rutherford backscattering study [43].

The measured ratio of the P 2p and Se 3d band intensities in the XPS spectrum is 1.1. We have deduced that the number of P atoms relative to the total number (250) of nanocrystal surface atoms is about 1.6. This indicates that there exist on the surface some additional TOPO molecules, which are not bound to the nanocrystals. This is somewhat surprising since the characteristic bands of the free TOPO molecules are observed neither in the FTIR (see figure 1) nor in the NMR spectra of the synthesized nanocrystal powder. The observation of an excess of TOPO molecules on the graphite surface may result from the spontaneous desorption of TOPO ligands from the nanocrystals in solution [42, 44] and from a higher sticking coefficient of TOPO molecules as compared to nanocrystals on the graphite surface [45]. For future experiments, we propose to solve the possible problem associated with the presence of free TOPO molecules in the nanocrystal solution, either by using very fresh nanocrystal solutions, where TOPO molecules have no time to desorb from the nanocrystals, or by replacing the TOPO molecules by more tightly bound ligands [46].

3.2.2. Deposition of NC on the hydrogenated Si(100) surface. We will now investigate the deposition of nanocrystals by the pulse injection method on the hydrogenated silicon surface, Si(100) 2 × 1:H. It is of particular interest to investigate the deposition of semiconductor nanocrystals on a semiconductor surface for the future use of such nanocrystals as optoelectronic nanodevices [7–10]. For example, the fluorescence of nanocrystals is expected to be quenched rapidly, when deposited on metallic or quasi-metallic surfaces. In contrast, when deposited on semiconductor surfaces, nanocrystals are expected to display very efficient fluorescence due to the reduced electronic relaxation of the nanocrystals by the surface [21]. Here, we have chosen to use the hydrogenated silicon Si(100) surface, since the hydrogen termination chemically passivates the surface. As a consequence, the solvent (pentane), which is evaporated in the UHV chamber when depositing a micro-droplet from the pulse valve, is expected to not react with the hydrogenated surface.

The hydrogenated Si(100) 2 × 1 surface has been prepared as described in [46]. The XPS spectra of the hydrogenated Si(100) surface before and after the injection of 12 pulses of the nanocrystal solution under UHV are shown in figures 6(a) and (b). After deposition, new photoemission bands associated with the Cd 3d, Se 3d, P 2p, P 2s and C 1s core levels are observed, as well as Auger electrons. The P 2p band is superimposed with a contribution from bulk silicon and the Se 3p band partly overlaps with the Si 2p bands.

A quantitative comparison with the deposition of nanocrystals on the graphite surface has been performed. From the relative intensities of the Se 3d photoemission bands in figure 7 (see the two lower curves), we have deduced that the nanocrystals have a similar sticking coefficient on graphite and hydrogenated Si(100).

3.2.3. Deposition of NC on the hydrogenated C(100) surface. As a final experiment, we have deposited nanocrystals by the pulse injection method on a hydrogenated diamond C(100) surface. Indeed diamond is a wide band gap (5.5 eV) material [47] transparent to visible light. This offers unique a opportunity for electronically exciting the nanocrystals [20] and exploiting their fluorescent properties.

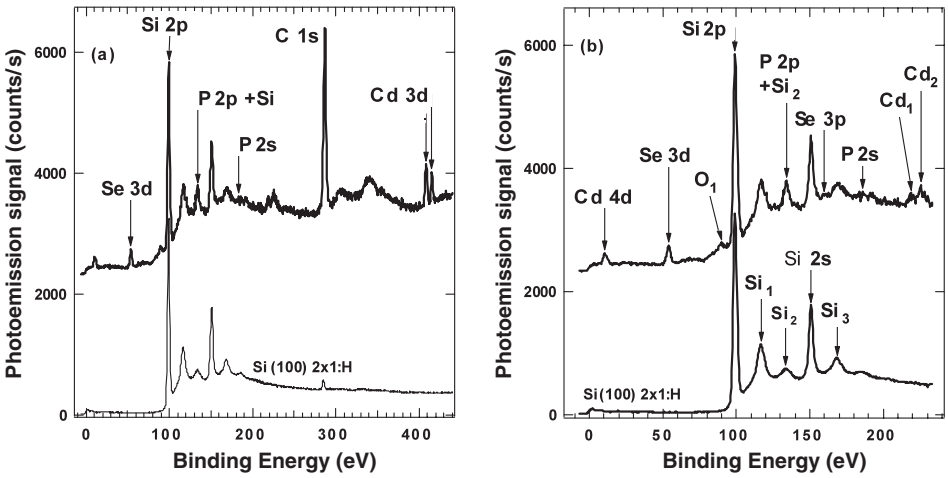

Figure 6. XPS spectra of the hydrogenated Si(100) 2 × 1 surface before (lower curve) and after (upper curve) injection of 24 pulses of the CdSe nanocrystal solution in pentane under UHV. The angle between the photon beam and the normal of the sample is 71.5°. The O_1, Cd_1 and Cd_2 bands are associated with the Auger electrons of oxygen and cadmium. The intensity of the XPS spectrum of the clean surface has been reduced for clarity. The binding energy extends up to 440 eV (a) and 230 eV (b).

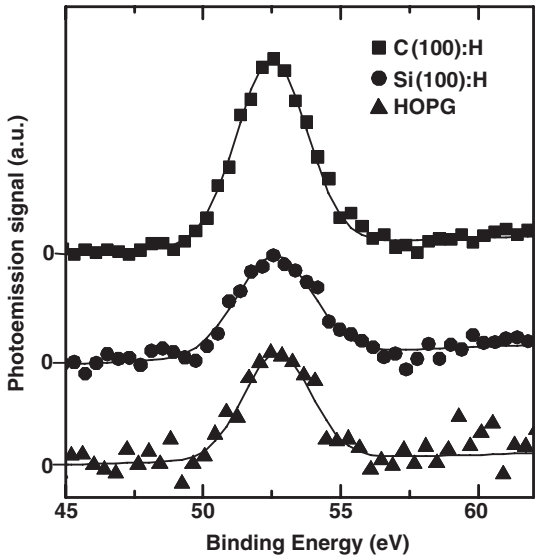

Figure 7. XPS spectra showing the Se 3d band after injection of four pulses of the CdSe nanocrystal solution in pentane under UHV on graphite (▲), hydrogenated Si(100) (●) and hydrogenated C(100) (■). The spectra have been shifted vertically for clarity. The photon energy is 600 eV.

A semiconducting boron-doped (type II b) natural single-crystal diamond with a polished (100) surface has been used. Sample preparation and hydrogenation of the C(100) surface have been described elsewhere [48]. The photoemission spectra at 600 eV of the hydrogenated diamond surface after the injection of 12 pulses of the nanocrystal solution under UHV are reported in figures 8(a) and (b). The presence of the Cd 4d, Cd 3d, Se 3d, Se 3p, P 2p and

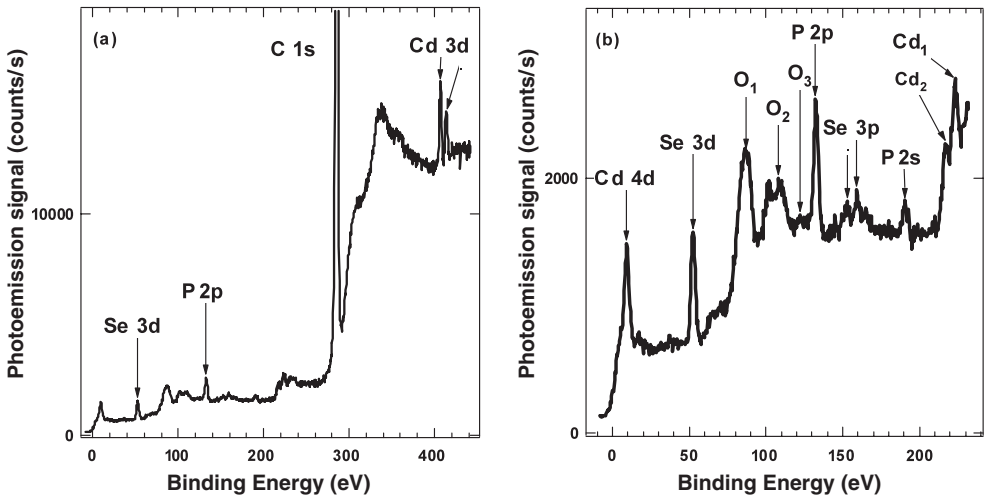

Figure 8. XPS spectra of the hydrogenated C(100) 2 × 1 surface, after injection of 12 pulses of the CdSe nanocrystal solution in pentane under UHV. The angle between the photon beam and the normal of the sample is 71.5°. The O_1, O_2, O_3, Cd_1 and Cd_2 bands are associated with the Auger electrons of oxygen and cadmium. The binding energy extends up to 440 eV (a) and 230 eV (b).

P 2s photoemission bands and of the Auger electrons of Cd indicates the adsorption of the nanocrystals on the hydrogenated diamond surface. The presence of the carbon chain of the ligands is revealed by the widening of the surface sensitive C 1s photoemission band recorded with 330 eV photons, and by the increased intensity of the surface resonance at 287.6 eV as observed in the NEXAFS spectrum (see figure 9).

The Se 3d photoemission bands recorded after four injection pulses on the hydrogenated Si(100) 2 × 1 and C(100) 2 × 1 surfaces are reported in figure 7. From this comparison, we deduce that nanocrystals have similar sticking coefficients on the two surfaces.

4. Conclusion

We have demonstrated that CdSe nanocrystals can be deposited on clean and well-ordered surfaces under ultrahigh vacuum conditions by using the pulse injection method. The sticking coefficient for the adsorption of CdSe nanocrystals has been found to be similar for the three surfaces investigated, namely HOPG, hydrogenated Si(100) 2 × 1 and hydrogenated C(100) 2 × 1.

In order to make the purity of the nanocrystal solutions compatible with the cleanliness of this new method of deposition, very pure solutions of CdSe nanocrystals have been prepared by a method derived from that of Peng *et al* [25, 26]. The CdSe nanocrystals studied (3 nm in diameter) have been found, after XPS analysis, to have a Cd rich surface with 74% Cd and 26% Se, in good agreement with NMR [42] and Rutherford backscattering results [43].

Interestingly, the XPS analysis has revealed a P/Se ratio larger than expected, thus implying the presence of additional TOPO molecules on the surface. As a solution for removing these 'free' TOPO molecules, we suggest the use of more tightly bound ligands [46].

In summary, we believe that the ability to deposit semiconductor nanocrystals on clean and well-ordered surfaces under ultrahigh vacuum conditions opens up exciting perspectives for investigating their electronic and optical properties with unprecedented reliability.

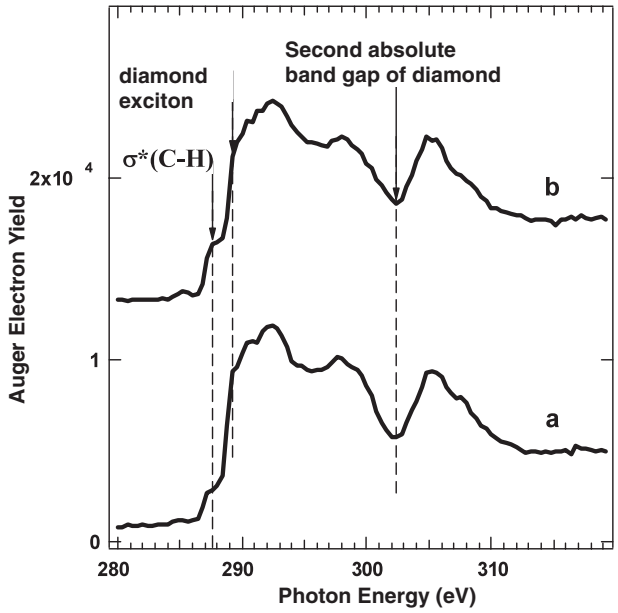

Figure 9. NEXAFS spectra of the hydrogenated C(100) surface before (a) and after (b) injection of 12 pulses of the CdSe nanocrystal solution in pentane under UHV vacuum. The energy of the electron analyser is set up at 254 eV. The energy window is 100 eV. The photon beam impinges at 71.5° onto the sample. The spectra have been normalized to the same photon flux.

Acknowledgments

We would like to thank S Gauthier and T Zambelli for fruitful discussions in designing the pulse injection experimental set-up. This work has been undertaken as part of an EU funded STREP 'Nanoman' (contract NMP4-CT-2003-550660) and the European RTN network 'AMMIST' (contract HPRN-CT-2002-00299).

Appendix A

Cadmium oxide (99.99%), selenium (99.999%), trioctylphosphine oxide (TOPO, technical, 90%) and trioctylphosphine (TOP, technical, 90%) were purchased from Aldrich and used as received. Octadecylphosphonic acid was purchased from Alpha-Aesar and used as received. Acetonitrile and toluene were purified by distillation over $CaCl_2$ and sodium/benzophenone respectively. All the synthetic and purification steps are realized under argon (nanocrystal solutions and solvents are handled by canulation; centrifuging is done in argon-flushed cells). Elemental selenium is handled in an argon-filled glove box.

The synthesis of 3 nm CdSe nanocrystals was realized according to a modified literature procedure, as discussed in section 2.1.

First step: synthesis of the selenium precursor.

Se (108 mg, 1.3 mmol), TOP (2 ml) and toluene (1 ml) are added into a Schlenck tube and kept under argon at 45 °C with vigorous stirring until complete dissolution of selenium occurs.

Second step: synthesis of the cadmium stearate precursor.

Tech. TOPO (40 g), stearic acid (0.719 g 2.6 mmol) and cadmium oxide (0.163 g 1.3 mmol) are loaded into a three-neck, round bottomed 250 ml flask fitted with a thermometer, a bubbling

system and a magnetic stirrer and connected to a vacuum line. The mixture is heated under a slow argon flow and vigorous stirring, and turns into a deep reddish suspension upon melting of the TOPO. Traces of oxygen are then removed by vacuum/argon flushing three times. The solution becomes colourless at 360 °C (complete reaction between cadmium oxide and stearic acid), and is then cooled to 245 °C.

Third step: growth of the nanocrystals.

The selenium solution is swiftly added to the cadmium stearate precursor at 245 °C. The temperature immediately drops to about 235 °C, and is kept at this value, while monitoring the growth of the crystals by UV–visible spectroscopy. After about 6 min, the heating system is removed, and the temperature decreases to 60 °C. Toluene (20 ml) is transferred under argon, and the flask is allowed to cool to ambient temperature. Acetonitrile (about 100 ml) is then slowly transferred under vigorous stirring to precipitate the nanocrystals as a fine orange suspension. The precipitate is transferred into a centrifuge cell (previously fitted with a rubber septum and flushed with argon) and centrifuged. The nearly colourless supernatant is discarded by canulation, and the crystals dissolved in toluene (8 ml) and centrifuged to remove any insoluble materials. The nanocrystal solution is then transferred into a second argon-flushed centrifuge cell, precipitated with 10 ml of acetonitrile and centrifuged again. The crystals are then subjected to three dissolution/precipitation cycles (8 ml toluene/10 ml acetonitrile respectively), dried under vacuum and stored at −23 °C under argon. The purity of the nanocrystal powder is checked by FTIR and NMR spectroscopy, and the characteristics of the nanocrystals in solution by absorption and fluorescence spectroscopy.

Appendix B

The photoelectrons detected from the different Cd (Se) atoms located inside a nanocrystal are those ejected along the axis of the analyser. As the diameter (d) of the nanocrystals has the same order of magnitude as the mean free path of the photoelectrons (λ), the photoelectrons contribute to the photoemission band, depending on the distance that they travel across the nanocrystal. Therefore, the intensity of a photoemission band associated with Cd (Se) bulk atoms is proportional to the number of Cd (Se) atoms inside the nanocrystal multiplied by an attenuation factor, A_B. Let us consider the core of a nanocrystal as a sphere of diameter d and, inside this sphere, let us consider a slice of width dx, perpendicular to the axis of the analyser and at a distance x from the centre of the sphere. The contribution of photoelectrons has to be weighted by

$$\frac{12}{3}\left[\int_0^{d/2} \mathrm{d}x \int_0^{\sqrt{\frac{d^2}{4}-x^2}} r\,\mathrm{d}r \exp\left(-\frac{\sqrt{R^2-r^2}-x}{\lambda}\right)\right.$$
$$\left. + \int_0^{d/2} \mathrm{d}x \int_0^{\sqrt{\frac{d^2}{4}-x^2}} r\,\mathrm{d}r \exp\left(-\frac{\sqrt{R^2-r^2}+x}{\lambda}\right)\right].$$

After integration, one derives the attenuation factor associated with the bulk atoms, which depends on the ratio λ/d:

$$A_B\left(\frac{\lambda}{d}\right) = \frac{3\lambda}{d} + \frac{6\lambda^2}{d^2}\mathrm{e}^{-\frac{d}{2\lambda}} - \frac{12\lambda^3}{d^3}(1-\mathrm{e}^{-\frac{d}{2\lambda}}) + 9\frac{\lambda^3}{d^3}$$
$$+ 3\left(\frac{\lambda^2}{d^2}+\frac{\lambda^3}{d^3}\right)\mathrm{e}^{-\frac{d}{\lambda}} - \frac{6\lambda^2}{d^3}(2\lambda+d)\,\mathrm{e}^{-\frac{d}{2\lambda}}.$$

The first three terms are the attenuation factors for atoms located in the upper half of the sphere of the nanocrystal core and the last three terms are for atoms located in the lower half

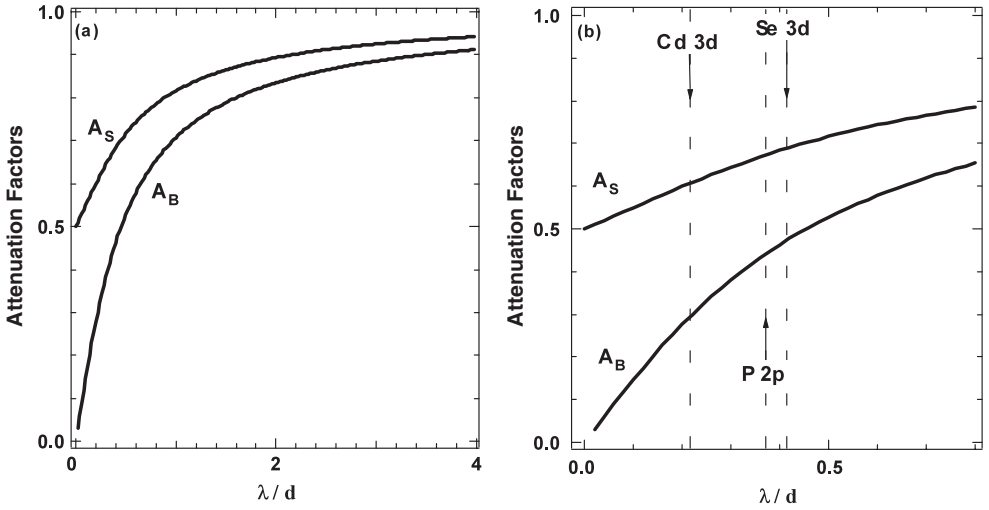

Figure B.1. Attenuation factors, A_B and A_S, of the photoemission bands associated with the core levels of bulk and surface atoms of a spherical nanocrystal as a function of the ratio λ/d. λ is the mean free path of the photoelectrons and d is the diameter of the nanocrystal. The ratio λ/d varies up to 4 (a) and 0.8 (b). In (b), the dotted lines are associated with Cd 3d, P 2p and Se 3d core levels and 3 nm nanocrystals.

of the sphere. The attenuation factor associated with the bulk atoms is given in figure B.1 as a function of λ/d. As expected, it increases with λ/d. The arrows indicate the attenuation factors associated with the observed Cd 4d, Cd 3d, Se 3d and Se 3s bands. The Cd (Se) atoms from the bottom half of the sphere contribute 18% (30%) to the Cd 3d (Se d) photoemission band.

Let us now consider the Cd (Se) atoms located at the surface of the nanocrystal. Their contribution to a photoemission band is weighted by the attenuation factor

$$A_S\left(\frac{\lambda}{d}\right) = \frac{1}{2}\left[1 + \frac{\lambda}{d}\left(1 - e^{-\frac{d}{\lambda}}\right)\right].$$

The attenuation factor associated with the atoms located at the surface of the nanocrystal is given in figure B.1 as a function of λ/d.

References

[1] Klein D L, Roth R, Lim A K L, Alivisatos A P and McEuen P L 1997 *Nature* **389** 699
[2] Kagan C R, Murray C B, Nirmal M and Bawendi M G 1996 *Phys. Rev. Lett.* **76** 1517
[3] Klimov V I, Mikhailovsky A A, Xu Su, Malko A, Hollingsworth J A, Leatherdale C A, Eisler H-J and Bawendi M G 2000 *Science* **290** 314
[4] Maenosono S, Ozaki E, Yoshie K and Yamaguchi Y 2001 *Japan. J. Appl. Phys.* **40** L638
[5] Kim B S, Islam M A, Brus L E and Herman I P 2001 *J. Appl. Phys.* **89** 8127
[6] Crooker S A, Hollingsworth J A, Tretiak S and Klimov V I 2002 *Phys. Rev. Lett.* **89** 186802
[7] Tessler N, Medvedev V, Kazes M, Kan S and Banin U 2002 *Science* **22** 1506
[8] Huynh W U, Dittmer J J and Alivisatos A P 2002 *Science* **295** 2425
[9] Coe S, Woo W-K and Bawendi M 2002 *Nature* **420** 800
[10] Tsutsui T 2002 *Nature* **420** 752
[11] Banin U, Cao Y, Katz D and Millo O 1999 *Nature* **400** 542
[12] Millo O, Katz D, Cao Y W and Banin U 2000 *Phys. Rev.* B **61** 16773
[13] Katz D, Millo O, Kan S-H and Banin U 2001 *Appl. Phys. Lett.* **79** 117

[14] Walzer K, Quaade U J, Ginger D S, Greenham N C and Stokbro K 2002 *J. Appl. Phys.* **92** 1434
[15] Bakkers E P A M and Vanmaekelbergh D 2000 *Phys. Rev.* B **62** 7743
[16] Alperson B, Rubinstein I, Hodes G, Porath D and Millo O 1999 *Appl. Phys. Lett.* **75** 1751
[17] Niquet Y M, Delerue C, Allan G and Lannoo M 2002 *Phys. Rev.* B **65** 165334
[18] Kanno T, Tannaka H, Nakamura T, Tabata H and Kawai T 1999 *Japan. J. Appl. Phys.* **38** L606
[19] Kasai H, Tanaka H, Okada S, Oikawa H, Kawai T and Nakanishi H 2002 *Chem. Lett.* **7** 696
[20] Terada Y, Choi B-K, Heike S, Fujimori M and Hashizume T 2003 *Japan. J. Appl. Phys.* **42** 4739
[21] Comtet G, Dujardin G, Hellner L, Lastapis M, Martin M, Mayne A J and Riedel D 2004 *Phil. Trans. R. Soc.* A **362** 1
[22] Klimov V I and Branch D W 1997 *Phys. Rev.* B **55** 13173
[23] Pokrant S and Whaley K B 1999 *Eur. Phys.* D **6** 255
[24] Murray C B, Kagan C R and Bawendi M G 2000 *Annu. Rev. Sci.* **30** 545
[25] Adam P Z and Peng X 2001 *J. Am. Chem. Soc.* **123** 183
[26] Qu L, Peng Z A and Peng X 2001 *Nano Lett.* **1** 333
[27] Reiss P, Bleuse J and Pron A 2002 *Nano Lett.* **2** 781
[28] Talapin D V, Rogach A L, Kornovski A, Haase M and Weller H 2001 *Nano Lett.* **1** 207
[29] Katari B J E, Colvin V L and Alivisatos A P 1994 *J. Phys. Chem.* **98** 4109
[30] Zingaro R 1963 *Inorg. Chem.* **2** 192
[31] Aldana J, Wang Y A and Peng X 2001 *J. Am. Chem.* **123** 8844
[32] Zambelli T, Jiang P, Lagoute J, Grillo S E, Gauthier S, Gourdon A and Joachim C 2002 *Phys. Rev.* B **66** 75410
[33] Beuhler R J, Flanigan E, Greene L J and Friedman L 1973 *J. Am. Chem. Soc.* **96** 3990
[34] Comtet G, Hellner L, Dujardin G and Ramage M J 1996 *Surf. Sci.* **352** 315
[35] Scofield J H 1976 *J. Electron Spectrosc.* **8** 128
[36] Davis L E, Mac Donald N C, Palmberg P W, Riach G E and Weber R E (ed) 1972 *Handbook of Auger Electron Spectroscopy* (Eden Prairie, USA: Physical Electronics Industries)
[37] Morar G J F, Himpsel F J, Hollinger G, Hughes G and McFeely F R 1986 *Phys. Rev.* B **33** 1340
[38] Comelli G, Stöhr J, Robinson C J and Jark W 1988 *Phys. Rev.* B **38** 7511
[39] Yeh J J and Lindau I 1985 Subshell photoionization cross sections *At. Data Nucl. Data Tables* **32** 1
[40] Powell C J, Jablonski A, Naumkin A, Krayt-Vass A, Conny J M and Rumble J R 2001 *J. Electron Spectrosc. Relat. Phenom.* **114** 1097
[41] Lide D R (ed) 1996–1997 *Handbook of Chemistry and Physics* 77th edn (Boca Raton, FL: CRC Press)
[42] Becerra L R, Murray C B, Griffin R G and Bawendi M G 1994 *J. Chem. Phys.* **100** 3297
[43] Taylor J, Kippeny T and Rosenthal S 2001 *J. Cluster Sci.* **12** 571
[44] Striolo A, Ward J, Prausnitz J M, Parak W J, Zanchet D, Gerion D, Milliron D and Alivisatos A P 2002 *J. Phys. Chem.* B **106** 5500
[45] Ge G and Brus L E 2001 *Nano Lett.* **1** 219
[46] Wang Y A, Li J J, Chen H and Peng X 2001 *J. Am. Chem. Soc.* **124** 2293
[47] Diederich L, Kuttel O M, Aebi P and Schlapbach L 1998 *Surf. Sci.* **418** 219
[48] Bobrov K, Comtet G, Dujardin G, Hellner L, Bergonzo P and Mer C 2001 *Phys. Rev.* B **63** 165421